Investigation of hole injection enhancement by MoO_3 buffer layer in organic light emitting diodes

Xu Haitao (徐海涛) and Zhou Xiang (周翔)[a)]
State Key Lab of Optoelectronic Materials and Technologies, Sun Yat-Sen University, Guangzhou 510275, People's Republic of China

(Received 23 October 2013; accepted 6 December 2013; published online 31 December 2013)

An MoO_3 buffer layer prepared by thermal evaporation as hole injection layer was investigated in organic light emitting diodes. The MoO_3 film inserted between the anode and hole transport layer decreased the operating voltage and enhanced power efficiency. Introduction of 1 nm MoO_3 film, which was found to be the optimum layer thickness, resulted in 45% increase in efficiency compared with traditional ITO anode. Results from atomic force microscopy and photoemission spectroscopy showed that smooth surface morphology and suitable energy level alignment of ITO/MoO_3 interface facilitated hole injection and transport. The hole injection and transport mechanism at the ITO/MoO_3 interface in thin and thick buffer layers were analyzed. © *2013 AIP Publishing LLC*.
[http://dx.doi.org/10.1063/1.4852835]

I. INTRODUCTION

Organic light emitting diodes (OLEDs) have attracted much attention in the past two decades because of their high efficiency, light weight, flexibility, and easy fabrication.[1–7] Achieving efficient hole injection is a fundamental topic in OLEDs. Indium tin oxide (ITO) is usually used as transparent conductive anode in OLEDs. The work function (WF) of as-grown ITO is 4.4 eV to 4.7 eV.[8–10] After oxygen plasma or UV-zone treatment, the WF of ITO anode can be increased to ~5.1 eV.[10] However, the highest occupied molecular orbital (HOMO) for hole-transport organic material is mostly >5.0 eV. For example, the HOMO of *N,N′*-[di(1-naphthyl)-*N, N′*-diphenyl]-1,1′-biphenyl-4,4′-diamine (NPB) is 5.4 eV. Therefore, the holes, which are injected from the ITO anode, have to overcome a large injection barrier. This barrier can be calculated from the energy level offset between the ITO Fermi level (E_F) and the HOMO of the hole transport layer (HTL). A large barrier results in high driving voltage and undesirable efficiency. Hence, modification of ITO electrode is needed to solve this problem.

Recent studies have reported that transition metal oxides (TMOs), including MoO_3,[12] WO_3,[13] V_2O_5,[14] and Fe_3O_4,[15] which are used as anode buffer layers, enhance device performance and long-term stability.[2] MoO_3, which has deep-lying energy band structure, is an *n*-type wide-bandgap TMO. Direct measurements, which were performed using UV photoemission spectroscopy (UPS) and inverse photoemission spectroscopy (IPES), of evaporated MoO_3 films showed that the edges of the conduction band (CB) and valance band (VB) of MoO_3 are 6.7 and 9.68 eV, respectively. The WF of MoO_3 film is adequately high (6.9 eV).[16,23,24] With the insertion of ultra-thin MoO_3 film between the ITOs and the HTL, the hole injection barrier was significantly reduced because of the high WF of MoO_3 films.[1] Some reports have analyzed the gap states in MoO_3 films to explain the injection barrier reduction. Given the appearance of reduced Mo atoms around the O vacancies in both evaporated and annealed MoO_3 films, the HOMO of NPB is at the highest gap state level of MoO_3, which is slightly under E_F, thereby leading to a small barrier.[17] Several schematic energy level diagrams at the interfaces have been established to elucidate the hole injection enhancement mechanism.[2,11,16,17] However, previous reports have considered a thin MoO_3 buffer layer. The hole injection process of thick MoO_3 buffer layer should be investigated further to fully understand the hole injection mechanism.

In this study, the MoO_3 buffer layer, which was used as an efficient hole injection layer (HIL), was prepared by thermal evaporation in OLEDs. With an optimized thickness of MoO_3 films, a 45% increase in efficiency was achieved compared with traditional ITO anode. Atomic force microcopy (AFM) and X-ray photoelectron spectroscopy (XPS) results show that smooth surface morphology and suitable energy level alignment of ITO/MoO_3 interface leads to efficient hole injection, thereby enhancing the performance efficiency. The hole injection and transport mechanism at the ITO/MoO_3 interface under thin and thick buffer layer conditions are discussed.

II. EXPERIMENTAL

All electroluminescence (EL) devices were fabricated using commercially purchased ITO substrates with sheet resistance of 10 Ω/□ by thermal evaporation. The configuration of EL devices was ITO/MoO_3 (*x* nm, where $x = 0$, 1, 3, 5, 10, 20)/NPB (40 nm)/tris(8-hydroxyquinoline) aluminum (Alq_3, 60 nm)/LiF (2.5 nm)/Al (100 nm). ITO substrates were sequentially ultrasonically cleaned using acetone, ethyl alcohol, and deionized water. After cleaning, the ITO substrates were dried using high-purity N_2 gas and baked for 15 min under ambient condition. EL devices were fabricated in the ultrahigh-vacuum (UHV) evaporation chamber at 2×10^{-8} Torr. Film thickness was monitored using a quartz

[a)]E-mail address: stszx@mail.sysu.edu.cn

TABLE I. Performance of the EL devices with different MoO_3 thicknesses.

Thickness of MoO_3 film (nm)	Turn-on voltage at 1 cd/m^2	Operating voltage at 1000 cd/m^2	Power efficiency (lm/W) at 50 mA/cm^2
0 (ref.)	4.3	8.5	1.31
1	2.4	4.7	1.92
3	2.4	5.2	1.78
5	2.4	5.5	1.78
10	2.4	5.6	1.65
20	2.4	6.0	1.42

crystal microbalance. The evaporation rates were carefully controlled at 1 and 0.2 Å/s for organic and inorganic materials, respectively. The EL properties were determined in ambient environment at room temperature without encapsulation. The current density–voltage–luminance (J–V–L) characteristics were measured using a Keithley SMU 236 source measure unit. The luminance characteristics were measured using a commercial luminance meter (ST-86LA, Photoelectric Instrument Factory of Beijing Normal University, China), which was equipped with a calibrated silicon photodiode. The key parameters of EL properties are summarized in Table I. In this study, the turn-on and operating voltages were defined as the applied voltage at 1 and 1000 cd/m^2, respectively.

The surface morphology was characterized using Benyuan CSPM5500 AFM under tapping mode at a scanning scale of $30 \times 30\ \mu m^2$. The surface roughness was calculated using Benyuan image analysis software.

To elucidate the chemical structure of MoO_3 films, XPS measurement was performed using VG ESCALAB 250 with monochromatic Al $K\alpha$ ($h\upsilon = 1486.6$ eV) radiation. The XPS spectral resolution was 0.05 eV. WF measurement was applied at a bias of -5 V to obtain the secondary-cutoff region. The MoO_3 films with varying thicknesses, which were prepared on ITO substrates, were transferred from the EL device fabrication chamber to the XPS analysis chamber. The transfer allowed air exposure for ~15 min.

III. RESULTS AND DISCUSSION

The current density–voltage, luminescence–voltage, and power efficiency–current density characteristics of the EL devices are shown in Fig. 1. In Fig. 1(a), the turn-on voltage of the reference device (ITO only) is 4.3 V. Compared with the reference device, the turn-on voltages of the MoO_3 devices with thicknesses from 1 nm to 20 nm maintained a constant value of 2.4 V. The operating voltage of the reference device is 8.5 V [Fig. 1(b)]. When the MoO_3 thickness is increased from 1 nm to 20 nm, the operating voltages first decreased from 8.5 V to 4.7 V, and then increased from 4.7 V to 6.0 V. Furthermore, the power efficiencies also increased from 1.31 lm/W to 1.92 lm/W [Fig. 1(c)] and then decreased from 1.92 lm/W to 1.42 lm/W at a current density of 50 mA/cm^2. Introduction of 1 nm MoO_3, which is the optimum value, results in 45% improvement in power efficiency. However, the turn-on voltage of MoO_3 modified devices fixed at 2.4 V shows that the similar energy level alignment is formed at anode/HTL interface, which will be

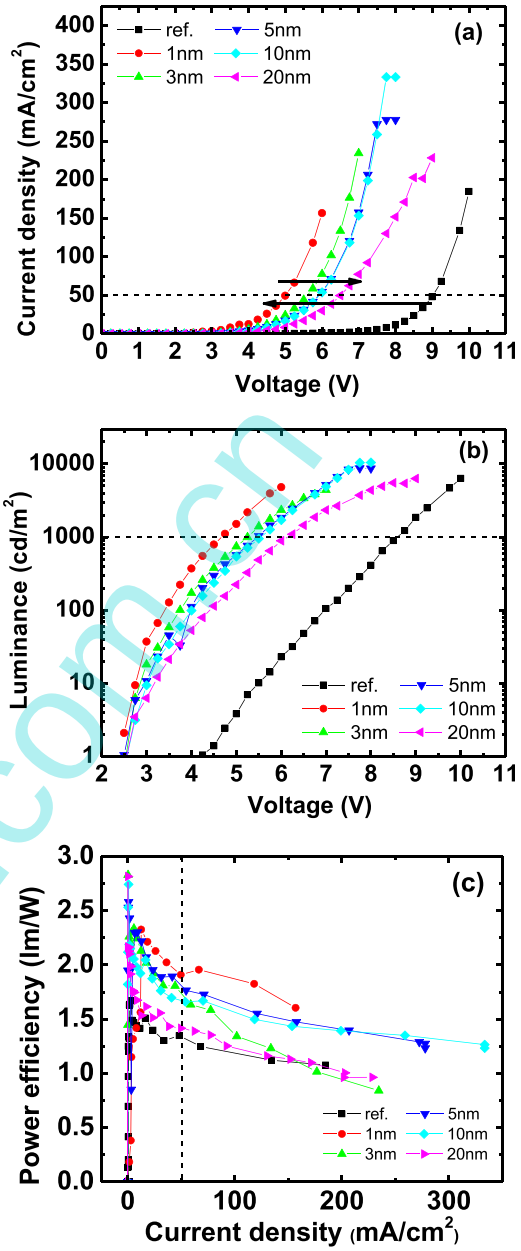

FIG. 1. (a) Current density–voltage, (b) luminance–voltage, (c) and power efficiency–current density characteristics of the devices.

presented later. On the other hand, a strong interfacial dipole layer (IDL) is formed at the MoO_3/NPB interface, which may lower the carrier injection, results in increase in operating voltage and decrease in power efficiency beyond the optimized buffer layer thickness.[2,11,17,25] Table I summarizes the performance parameters for the EL devices with varying thicknesses from 0 nm to 20 nm. These results indicate that superior hole injection and transport, caused by the introduction of MoO_3 buffer layer, results in considerable enhancement in EL device performance.

To obtain more information on the effect of MoO_3 buffer layer on the performance enhancement, AFM tests were performed on the surface of the ITO and ITO/MoO_3 films. The AFM images of the MoO_3 films, which show the surface formation and roughness, are depicted in Fig. 2. MoO_3 grains are found on the ITO/MoO_3 substrates. Each ITO/MoO_3 film

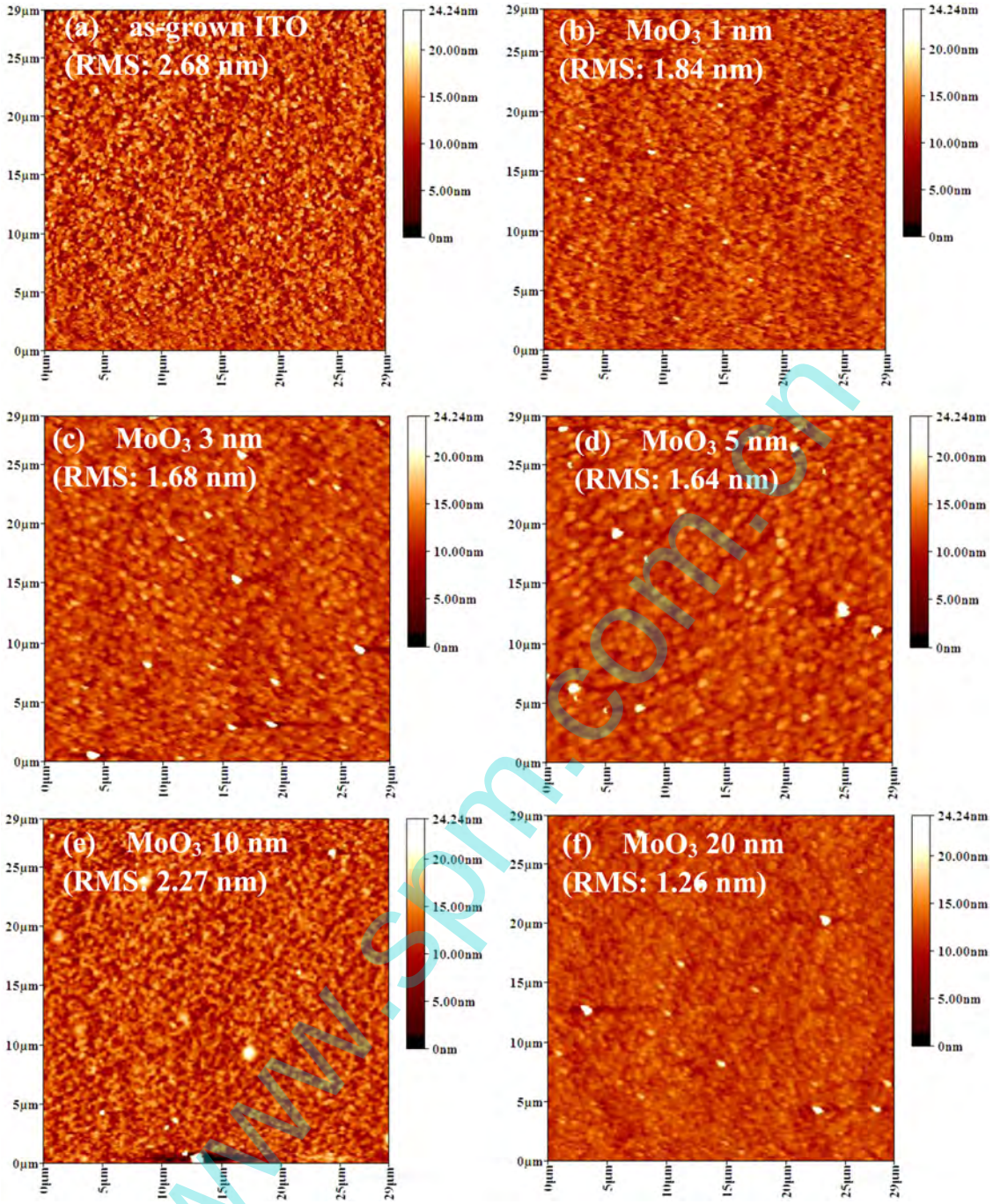

FIG. 2. AFM images of MoO_3 films with different thicknesses.

shows a uniform surface, with root mean square (RMS) roughness values ranging from 1.26 nm to 2.27 nm. Compared with MoO_3 surface, the ITO substrate shows an RMS roughness of 2.68 nm. The difference in the RMS values of the ITO and ITO/MoO_3 surfaces implies that the deposition of MoO_3 results in a homogeneous film surface. Therefore, the deposited MoO_3 films are smooth enough to improve the interfacial contact between ITO and HTL.

To determine the energy level alignment, the relations between MoO_3 thickness and binding energy of vacuum level (VL), CB minimum (CBM), raising edge of gap states, and VB maximum (VBM) from the XPS VB spectra and secondary-cutoff spectra are summarized in Fig. 3. The CBM was calculated using the VBM and the band gap of MoO_3 (3.2 eV).[18,21] The observed data of VBM, in which the edge of gap states and CBM are increased, are consistent with the references.[17,23,24] The WF values of MoO_3 films, which were calculated from the offset of VL and E_F, remarkably increased from 4.5 eV to 5.2 eV. This result implies that the hole injection barrier at the anode/HTL interface can be considerably decreased by the improvement of WF. Given that air exposure lowers the measured WF of evaporated MoO_3 films, the observed WF values are slightly lower than that in the references.[23,24] However, in EL device fabrication, the MoO_3 buffer layer maintains a high WF at UHV without breaking the vacuum to achieve little hole injection

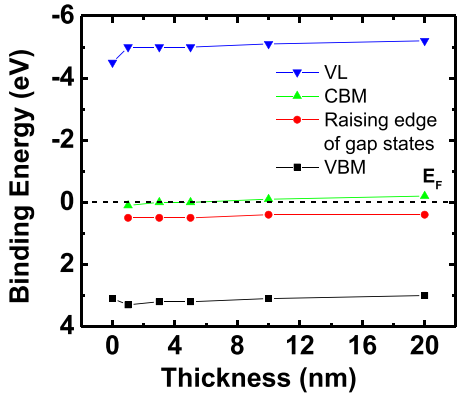

FIG. 3. Binding energy versus MoO_3 layer thickness for the energy level alignment at vacuum level (blue triangle), CBM (green triangle), increased edge of gap states (red circle), and VBM (black square).

barrier. Moreover, CBM is very close to E_F, and the increase in edge of gap states is slightly lower than the E_F, thereby indicating that electrons at gap states are easily excited to CBM. The energy level alignment implies that holes can be transferred via gap states and electrons can be transferred via CB.[16,17]

To elucidate the chemical structures of the evaporated MoO_3 films, XPS measurements of the MoO_3 films deposited on ITO substrates were performed. The MoO_3 thickness dependence of the XPS spectra is shown in Fig. 4. The Mo 3*d* core level spectra are shown in Fig. 4(a). The doublet of Mo3*d*5 and Mo3*d*3, which are attributed to the Mo +6 species,[17,19,20] are observed at 233.2 and 236.3 eV, respectively. The binding energies of Mo +6 doublet are almost constant in the core level spectra, regardless of film thickness, which indicates that the change in MoO_3 thickness does not cause charge transfer. In the 1 nm spectrum, a shoulder, which indicates another species of Mo in evaporated MoO_3 films, appears at low binding energies. A secondary Mo 3*d* doublet (Mo3*d*5 at 232 eV and Mo3*d*3 at 235.2 eV) indicates that Mo +5 species are obtained as determined by the fitting analysis for all of the MoO_3 films.[19,20] This phenomenon indicates that oxygen vacancies exist in the evaporated MoO_3 films, resulting in reduced Mo atoms. From the fitting data, the calculated Mo–O ratios are 2.95, 2.96, 2.97, 2.97, 2.97, and 2.98, which correspond to the film thickness. The reduced Mo atoms lead to gap states caused by the partial filling of unoccupied Mo 4*d* levels.[11,17] The In 3*d* core level spectra, which indicate the MoO_3 film cover, are shown in Fig. 4(b). The signal areas in In 3*d* are considerably diminished with increasing MoO_3 thickness. This result suggests that continuous film formations are achieved in $\geq$10-nm thick MoO_3 films. Thinner MoO_3 films are discontinuous because of the formation of grains or clusters, without covering all of the ITO substrates.

The hole injection and transport mechanism of MoO_3 buffer layer are discussed under thin or thick buffer layer conditions. Based on the characteristics of the EL devices and XPS results, the schematic energy level alignment of the MoO_3 buffer layer is shown in Fig. 5. The XPS results show that the hole injection enhancement is due to the high WF and *n*-type semiconducting property of MoO_3. When MoO_3 buffer layer is introduced in EL devices, the high WF causes

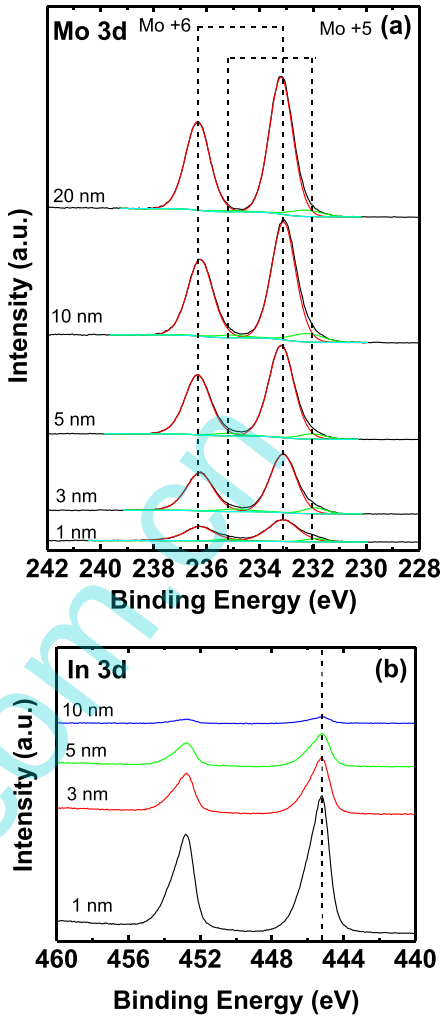

FIG. 4. XPS spectra for (a) Mo 3*d* and (b) In 3*d* of MoO_3 films with different thicknesses.

dipoles at the ITO/MoO_3 and MoO_3/NPB interfaces.[11,17] The interfacial dipole rearranges the energy level alignment of anode and HTL to benefit hole injection and transport. The CBM and gap states of MoO_3, well as the HOMO of NPB, are very close to E_F, which is suitable to the hole injection from anode to HTL. Several studies have reported on the relative interfacial energy level alignment using XPS measurements.[16–18] Therefore, the hole injection barrier is significantly reduced by the energy level rearrangement. When a thin MoO_3 buffer layer is used (Fig. 5, left), the holes are directly injected into the HOMO of NPB via tunneling from anode through MoO_3 buffer layer. By contrast, when a thick layer is used, the injection passes through the CBM and gap states (Fig. 5, right). First, the electrons are transferred from the HOMO of NPB to CBM of MoO_3 by the internal electric field, which is due to the MoO_3/NPB interfacial dipole. Given the external bias, the electrons at CBM of MoO_3 and the holes at the HOMO of NPB are driven towards the corresponding opposite electrodes. Moreover, the process repeats at positive bias. This process is also called charge generation and separation.[16,22] Through this process, the hole injection current is converted to electron current by the MoO_3/NPB interface. Even though MoO_3

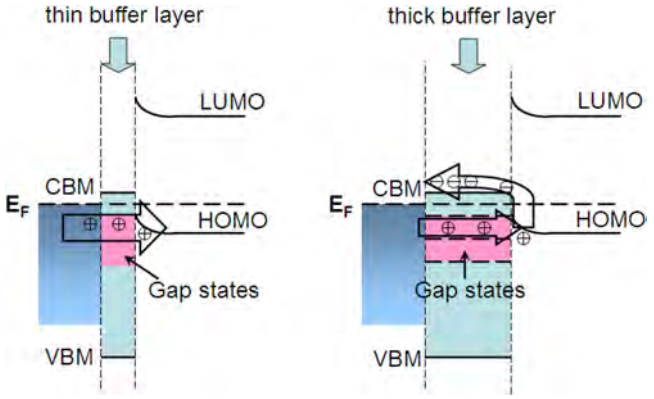

FIG. 5. Schematic energy level alignment of the hole injection and transport of MoO_3 buffer layer in thin or thick model.

is once considered to have an insulator-like property with a large forbidden gap of 3.2 eV, the EL devices can achieve enough driven current using a thick MoO_3 layer. Furthermore, while using optimized buffer layer thickness, an appropriate charge generation rate occurs at MoO_3/NPB interface, results in the best charge injection and power efficiency. On the other hand, while using thicker buffer layer, an excess charge generation rate is generated due to the efficient charge transfer, results in a strong space charge layer in NPB, which may lower the charge injection and reduce the power efficiency.[22] Second, the gap states in MoO_3 are also important in hole injection and transport. The holes are transferred from the ITO anode to the HTL via gap states. However, according to the XPS fitting results, an increase in Mo–O ratios results in maintained low density of gap states in MoO_3 films. Thus, the hole injection current through gap states is restricted in thick MoO_3 films. This result suggests that the hole injection current is maintained partially by the charge generation and separation process at the MoO_3/NPB interface and partially by the charge transfer passing through the gap states in MoO_3.

IV. SUMMARY AND CONCLUSIONS

The MoO_3 buffer layer is analyzed in Alq-based OLEDs. The J-V-L characteristics of the MoO_3 devices show reduced operating voltage and enhanced performance in terms of power efficiency. Introduction of 1 nm MoO_3 film, which is the optimum film thickness, results in 45% increase in efficiency compared with that of traditional ITO anode. AFM tests show that smooth morphology may result in better interfacial contact between ITO and HTL. The XPS measurements also demonstrate that high WF and suitable energy level alignment of ITO/MoO_3 interface are beneficial for the hole injection in MoO_3 devices. According to the energy level alignment, we suggest a hole injection mechanism of MoO_3 buffer layer in thin and thick buffer layers. Direct hole injection via carrier tunneling is the main process when thin MoO_3 buffer layer is used. By contrast, hole injection paths pass through the CBM and gap states when a thick layer is used. The charge generation and separation process at the MoO_3/NPB interface and gap states of MoO_3 are important in hole injection and transport.

ACKNOWLEDGMENTS

This work was supported by the National Natural Science Foundation of China (11274402), the Doctoral Foundation from Ministry of Education (20100171110025), the State Key Laboratory of Optoelectronic Materials and Technologies (2010-RC-3-1).

[1]H. You, Y. F. Dai, Z. Q. Zhang, and D. G. Ma, J. Appl. Phys. **101**, 026105 (2007).
[2]F. X. Wang, X. F. Qiao, T. Xiong, and D. G. Ma, Org. Electron. **9**, 985–993 (2008).
[3]C. Lin, C. Yeh, M. Chen, S. Hsu, C. Wu, and T. Pi, J. Appl. Phys. **107**, 053703 (2010).
[4]W. Cao, Y. Zheng, Z. Li, E. Wrzesniewski, W. T. Hammond, and J. Xue, Org. Electron. **13**, 2221–2228 (2012).
[5]P.-S. Wang, Y.-Y. Lo, W.-H. Tseng, M.-H. Chen, and C.-I. Wu, J. Appl. Phys. **114**, 063710 (2013).
[6]S.-W. Seo, E. Jung, S. J. Seo, H. Chae, H. K. Chung, and S. M. Cho, J. Appl. Phys. **114**, 143505 (2013).
[7]L. Zhou, J. Y. Zhuang, S. Tongay, W. M. Su, and Z. Cui, J. Appl. Phys. **114**, 074506 (2013).
[8]Q. T. Le, F. Nuesch, L. J. Rothberg, E. W. Forsythe, and Y. Gao, Appl. Phys. Lett. **75**, 1357–1359 (1999).
[9]V. Christou, M. Etchells, O. Renault, P. J. Dobson, O. V. Salata, G. Beamson, and R. G. Egdell, J. Appl. Phys. **88**, 5180–5187 (2000).
[10]H. Y. Yu, X. D. Feng, D. Grozea, and Z. H. Lu, Appl. Phys. Lett. **78**, 2595–2597 (2001).
[11]H. Lee, S. W. Cho, K. Han, P. E. Jeon, C. Whang, K. Jeong, K. Cho, and Y. Yi, Appl. Phys. Lett. **93**, 043308 (2008).
[12]M. Kröger, S. Hamwi, J. Meyer, T. Riedl, W. Kowalsky, and A. Kahn, Org. Electron. **10**, 932–938 (2009).
[13]M. J. Son, S. Kim, S. Kwon, and J. W. Kim, Org. Electron. **10**, 637–642 (2009).
[14]J. Meyer, K. Zilberberg, T. Riedl, and A. Kahn, J. Appl. Phys. **110**, 033710 (2011).
[15]D. Zhang, J. Feng, Y. Liu, Y. Zhong, Y. Bai, Y. Jin, G. Xie, Q. Xue, Y. Zhao, S. Liu, and H. Sun, Appl. Phys. Lett. **94**, 223306 (2009).
[16]M. Kröger, S. Hamwi, J. Meyer, T. Riedl, W. Kowalsky, and A. Kahn, Appl. Phys. Lett. **95**, 123301 (2009).
[17]K. Kanai, K. Koizumi, S. Ouchi, Y. Tsukamoto, K. Sakanoue, Y. Ouchi, and K. Seki, Org. Electron. **11**, 188–194 (2010).
[18]Irfan, H. Ding, Y. Gao, D. Y. Kim, J. Subbiah, and F. So, Appl. Phys. Lett. **96**, 073304 (2010).
[19]P. Wang, I. Wu, W. Tseng, M. Chen, and C. Wu, Appl. Phys. Lett. **98**, 173302 (2011).
[20]J. J. Jasieniak, J. Seifter, J. Jo, T. Mates, and A. J. Heeger, Adv. Funct. Mater. **22**, 2594–2605 (2012).
[21]Irfan, H. Ding, Y. Gao, C. Small, D. Y. Kim, J. Subbiah, and F. So, Appl. Phys. Lett. **96**, 243307 (2010).
[22]T. Matsushima and H. Murata, Appl. Phys. Lett. **95**, 203306 (2009).
[23]S. R. Hammond, J. Meyer, N. E. Widjonarko, P. F. Ndione, A. K. Sigdel, A. Garcia, A. Miedaner, M. T. Lloyd, A. Kahn, D. S. Ginley, J. J. Berry, and D. C. Olson, J. Mater. Chem. **22**, 3249–3254 (2012).
[24]J. Meyer, S. Hamwi, M. Kröger, W. Kowalsky, T. Riedl, and A. Kahn, Adv. Mater. **24**, 5408–5427 (2012).
[25]T. Matsushima, Y. Kinoshita, and H. Murata, Appl. Phys. Lett. **91**, 253504 (2007).